

# **Entropy and optimality in river deltas**

Alejandro Tejedor<sup>a</sup>, Anthony Longjas<sup>a</sup>, Douglas A. Edmonds<sup>b,c</sup>, Ilya Zaliapin<sup>d</sup>, Tryphon T. Georgiou<sup>e</sup>, Andrea Rinaldo<sup>f,g,1</sup>, and Efi Foufoula-Georgiou<sup>a,1</sup>

<sup>a</sup>Department of Civil and Environmental Engineering, University of California, Irvine, CA 92697; <sup>b</sup>Department of Earth and Atmospheric Sciences, Indiana University, Bloomington, IN 47405; Center for Geospatial Data Analysis, Indiana University, Bloomington, IN 47405; Department of Mathematics and Statistics, University of Nevada, Reno, NV 89557; Department of Mechanical and Aerospace Engineering, University of California, Irvine, CA 92697; fLaboratory of Ecohydrology, Ecole Polytechnique Federale Lausanne, 1015 Lausanne, Switzerland; and <sup>9</sup>Dipartimento di Ingegneria Civile, Edile ed Ambientale, Università di Padova, 35131 Padova, Italy

Contributed by Andrea Rinaldo, August 29, 2017 (sent for review May 22, 2017; reviewed by Axel Kleidon and John B. Shaw)

The form and function of river deltas is intricately linked to the evolving structure of their channel networks, which controls how effectively deltas are nourished with sediments and nutrients. Understanding the coevolution of deltaic channels and their flux organization is crucial for guiding maintenance strategies of these highly stressed systems from a range of anthropogenic activities. To date, however, a unified theory explaining how deltas self-organize to distribute water and sediment up to the shoreline remains elusive. Here, we provide evidence for an optimality principle underlying the self-organized partition of fluxes in delta channel networks. By introducing a suitable nonlocal entropy rate (nER) and by analyzing field and simulated deltas, we suggest that delta networks achieve configurations that maximize the diversity of water and sediment flux delivery to the shoreline. We thus suggest that prograding deltas attain dynamically accessible optima of flux distributions on their channel network topologies, thus effectively decoupling evolutionary time scales of geomorphology and hydrology. When interpreted in terms of delta resilience, high nER configurations reflect an increased ability to withstand perturbations. However, the distributive mechanism responsible for both diversifying flux delivery to the shoreline and dampening possible perturbations might lead to catastrophic events when those perturbations exceed certain intensity thresholds.

spectral graph theory | information theory | self-organization | resilient deltas

River deltas are depositional landforms forming downstream of major rivers, often home to large populations and important natural resources (1-10). In the last decades, many deltas of the world have been under threat from a range of stressors, including sea-level rise, upstream dam development, and local exploration (2, 4, 5, 11–17). Deltas are nourished by channel networks whose connectivity constrains, if not drives, the evolution, functionality, and resilience of these systems. Remarkably, the properties of delta channel networks differ substantially from the tree-like topology of the rivers that feed them (18). Tree-like networks, defined by the absence of loops, are characteristic of tributary river networks and are found abundantly in nature across different systems and scales (e.g., botanical trees, veins of leaves, blood vessels, lightning, and river networks). The propensity of nature in choosing tree-like configurations has been grounded as an optimality principle. Specifically, tributary river channel networks achieve minimal total energy dissipation, that is, minimal loss of potential energy as water and sediment flow downstream, albeit often manifesting as feasible optimality, that is, a dynamically accessible local minimum due to initial conditions and other constraints (19-22). Similar to river networks, vascular networks in biological systems (e.g., animals, plants, insects, etc.), which transport materials through space filling fractal networks of branching tubes, achieve states of minimal energy dissipation (23, 24). Analogous optimality principles have also been suggested to constrain processes as diverse as root water uptake in plants (minimization of internal dissipation) (25) and

land surface energy and water balance (maximization of power) (26-28).

Despite the importance of deltaic systems and the recent advances in quantifying their connectivity properties (18, 29–34), an optimality principle for the organization of their distributary channel networks, akin to that existing for the tributary networks, remains elusive. A recent framework based on spectral graph theory (29, 30, 32) sheds light on the topologic and steady-state flux partitioning characteristics of delta channel networks and their relationship to underlying morphodynamic controls (e.g., sediment composition and tidal and wave energy), paving the way for quantitative delta classification and inference of process from form. However, the diversity of topologic structures of channel networks across a broad spectrum of deltas, and the fact that deltas are highly dynamic systems within which topology and flux partition coevolve, make it challenging to find a universal firstorder optimality principle (e.g., minimization of energy, maximization of entropy, or minimization of free energy) governing their formation.

We are physically motivated by the foundational principle that deltas build land by spreading their fluxes on their delta top, as opposed to creating single pathways to the ocean which would diminish the formation of islands that retain sediment and nutrients and reduce land-building potential. This notion resonates with previous results applied to tidal deltas showing that tidal channels self-organize to uniformly distribute the tidal prism across the delta (35). Under this premise, we postulate the

### Significance

River deltas are critically important Earthscapes at the landwater interface, supporting dense populations and diverse ecosystems while also providing disproportionately large food and energy resources. Deltas exhibit complex channel networks that dictate how water, sediment, and nutrients are spread over the delta surface. By adapting concepts from information theory, we show that a range of field and numerically generated deltas obey an optimality principle that suggests that deltas self-organize to increase the diversity of sediment transport pathways across the delta channels to the shoreline. We suggest that optimal delta configurations are also more resilient because the same mechanism that diversifies the delivery of fluxes to the shoreline also enhances the dampening of possible perturbations.

Author contributions: A.T., A.L., D.A.E., I.Z., T.T.G., A.R., and E.F.-G. designed research. performed research, analyzed data, and wrote the paper.

Reviewers: A.K., Max Planck Institute for Biogeochemistry; and J.B.S., University of Arkansas.

The authors declare no conflict of interest.

Freely available online through the PNAS open access option.

<sup>1</sup>To whom correspondence may be addressed. Email: andrea.rinaldo@epfl.ch or efi@uci.edu.

This article contains supporting information online at www.pnas.org/lookup/suppl/doi:10. 1073/pnas.1708404114/-/DCSupplemental.

existence of an optimality principle in delta channel networks in terms of achieving configurations that maximize the diversity of flux delivery from any point of the network to the shoreline. The time scale of topologic reorganization in deltas, which is mainly through major channel avulsions, is of the order of decades to millennia, depending on the deltaic system (36, 37), whereas the flux adaptation on a given channel topology has a characteristic time scale which is orders of magnitude smaller. This separation of scales allows us to study the system on a fixed topology and focus on whether an optimality principle governs the distribution of fluxes on that topology.

Given the nature of our hypothesis, that is, maximization of the diversity (or uncertainty) of flux delivery from any point of the network to the shoreline, we adopt an information theoretic approach to quantify uncertainty based on Shannon entropy (38). Note that Jaynes (39) introduced a formalism demonstrating the equivalence (under thermodynamic equilibrium) of the statistical mechanics and information theory approach to entropy. Furthermore, it has been argued (not exempt from certain controversy) that the mathematical framework formulated by Jaynes (39) serves as a generalization of the statistical mechanics framework for both equilibrium and nonequilibrium systems (40, 41). In this work, we propose the notion of nonlocal entropy rate (nER) and suggest by comparative analysis of field and numerical deltas that indeed deltas self-adjust their flux partition so that they maximize their flux diversity. Note that by "maximization" we do not refer to a global optimization, that is, deltas generally do not achieve flux configurations that correspond to the absolute maximum value of nER but exhibit configurations corresponding to dynamically accessible (local) maximum (feasible optimality). We also discuss the possible implications of the proposed optimality principle with respect to delta resilience in response to perturbations, arguing that flux distributions characterized by extreme values of nER are more resilient, in that a local perturbation (e.g., flux reduction in a channel) will affect the least the distribution of fluxes at the shoreline outlets.

#### Nonlocal Entropy Rate (nER)

Entropy quantifies the uncertainty in the occurrence of events (38), that is, the amount of information needed to describe the outcome of an experiment. Uncertainty intuitively emerges from the notions of probability and surprise. For instance, given a discrete stochastic process  $\{X_i\}$ , such as rolling a six-sided die, with specified probability distribution of outcomes, for example  $\{p_1, p_2, ..., p_6\}$ , the occurrence of rolling a 3 when all sides are numbered 3 produces zero surprise. Conversely, on the same die rolling a number other than 3 would produce infinite surprise. Mathematically, this surprise is defined as  $-\log(p_i)$ . Therefore, the uncertainty of an event,  $h_i$ , is the product of  $-\log(p_i)$ times its probability of occurrence  $p_i$ . Thus, either the occurrence of a completely certain event  $(p_i = 1)$  or an impossible one  $(p_i = 0)$  introduces zero uncertainty  $(h_i = 0, by convention)$  $0 \log 0 = 0$ ). The uncertainty is maximal when all of the N possible outcomes have the same probability of occurrence 1/N (e.g., fair die where the number on each face has a probability of occurrence 1/6). The total uncertainty or entropy, H, of a set of N discrete outcomes with probabilities  $\{p_1, p_2, ..., p_i, ..., p_N\}$  is equal to the sum of the uncertainties corresponding to each outcome i (42):

$$H = \sum_{i}^{N} h_i = -\sum_{i}^{N} p_i \log p_i.$$
 [1]

We aim to develop an entropic metric for delta channel networks that quantifies the diversity of flux delivery to the shoreline. Thus, a delta channel network with low entropy, that is, with low uncertainty in flux pathways, would be one with a dominant channel that carries most of the flux. This configuration is inherently unstable, assuming no redistribution of sediment by marine processes, because that channel would prograde until its water slope reduces and the channel avulses down a steeper path (43, 44). However, a delta channel network that achieves a configuration where all of the possible pathways that drain water and

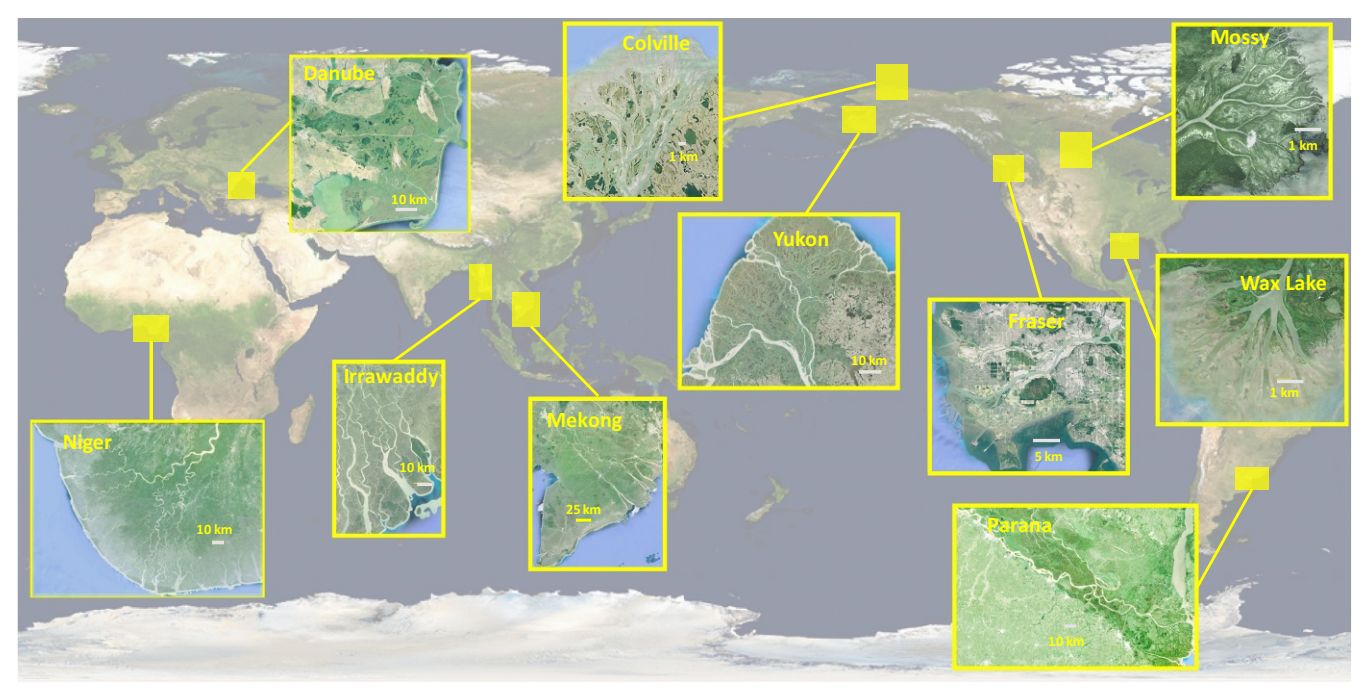


Fig. 1. Field deltas and their corresponding location. Ten deltas with diverse morphodynamic environments and of various degrees of channel complexity were analyzed in terms of their nER (see SI Appendix for further details about the deltas). Satellite images provided by Landsat/Copernicus, NASA, Digital Globe, and CNES/Airbus were extracted from Google Earth. We acknowledge their respective copyrights.

sediment from any point of the network to the shoreline are equally probable would have the highest entropy. This uncertainty in delivery would have the stabilizing effect of spreading sediment evenly across the shoreline. Notice that maximizing the uncertainty of water and sediment flux delivery to the shoreline does not necessarily imply networks that proportion fluxes equally at every single bifurcation. In fact, this would be inconsistent with morphodynamic theories (45, 46) which showed that asymmetric flux partition at a junction is a requirement for stability.

Conceptualizing delta channel networks as graphs, where nodes correspond to junctions or bifurcations, and links represent channels ( $Materials\ and\ Methods$ ), we define a metric of uncertainty of water and sediment flux pathways from the node i to the shoreline as

$$h_i^{NL} = -\sum_k p_{ik} \log p_{ik},$$
 [2]

where  $p_{ik}$  is the transition probability from node i to outlet node k. Alternatively,  $p_{ik}$  represents the fraction of water and sediment flux from node i that eventually drains to outlet k (see Materials and Methods for details on the computation of  $p_{ik}$ ). We refer to  $h_i^{NL}$  as the nonlocal entropy for node i, to emphasize that the transition probabilities are between nodes i and the shoreline nodes k as opposed to among neighboring nodes (local). This notion acknowledges important nonlocal effects on delta dynamics, such as the hydrodynamic backwater where the water surface slope is dependent on the water depth at the shoreline and the local slope between subsequent bifurcations (36, 44).

By weighing  $h_i^{NL}$  with the normalized steady-state flux at each node  $\pi_i$  ( $\sum_i \pi_i = 1$ ), we define the nER of the complete delta channel network:

$$nER = \sum_{i} \pi_{i} \frac{h_{i}^{NL}}{h_{i,max}^{NL}} = \sum_{i} \pi_{i} \frac{\sum_{k} p_{ik} \log p_{ik}}{\log \frac{1}{N_{i}}},$$
 [3]

where  $h_{i,max}^{NL} = -\log\frac{1}{N_i}$  is a normalization factor computed for each node i and  $N_i$  represents the number of outlet nodes that can be reached from node i. The normalized nER admits values in the interval [0,1].

#### **Results and Discussion**

We hypothesize that deltas distribute the flux at each bifurcation to maximize the uncertainty in the delivery of fluxes from any point of the delta to the shoreline, that is, to achieve a dynamically accessible maximum of nER. We computed the nER for 10 deltas with diverse morphodynamic environments and channel complexity (Fig. 1; see SI Appendix for the extracted channel networks and physical information about the deltas). We compared the computed nER for each field delta (based on the actual flow partitions) against 105 randomizations of the flux partition at each bifurcation [sampled from a uniform distribution in the interval (0,1)] holding the network structure constant. Despite the broad range of climate, discharge, and sediment influencing these deltas, all but one (the Niger delta) have flux configurations that exhibit extreme values of nER, that is, 9 of 10 field deltas have nER above the 90th percentile of the random distribution (probability of exceedance  $P_E < 0.1$ ) (Fig. 2). The fact that the computed value of nER does not correspond to the absolute maximum of the distribution is not surprising. Natural systems have been argued to achieve stationary configurations that do not correspond to the absolute optimum of the functional describing their organizational principle but to local optima that are accessible given the initial conditions, constraints, and the system dynamics, known as the feasible optimality principle (19-22). Beyond field deltas, we also applied the nER analysis to numerically simulated deltas that formed under varying incoming sediment grain sizes (32,

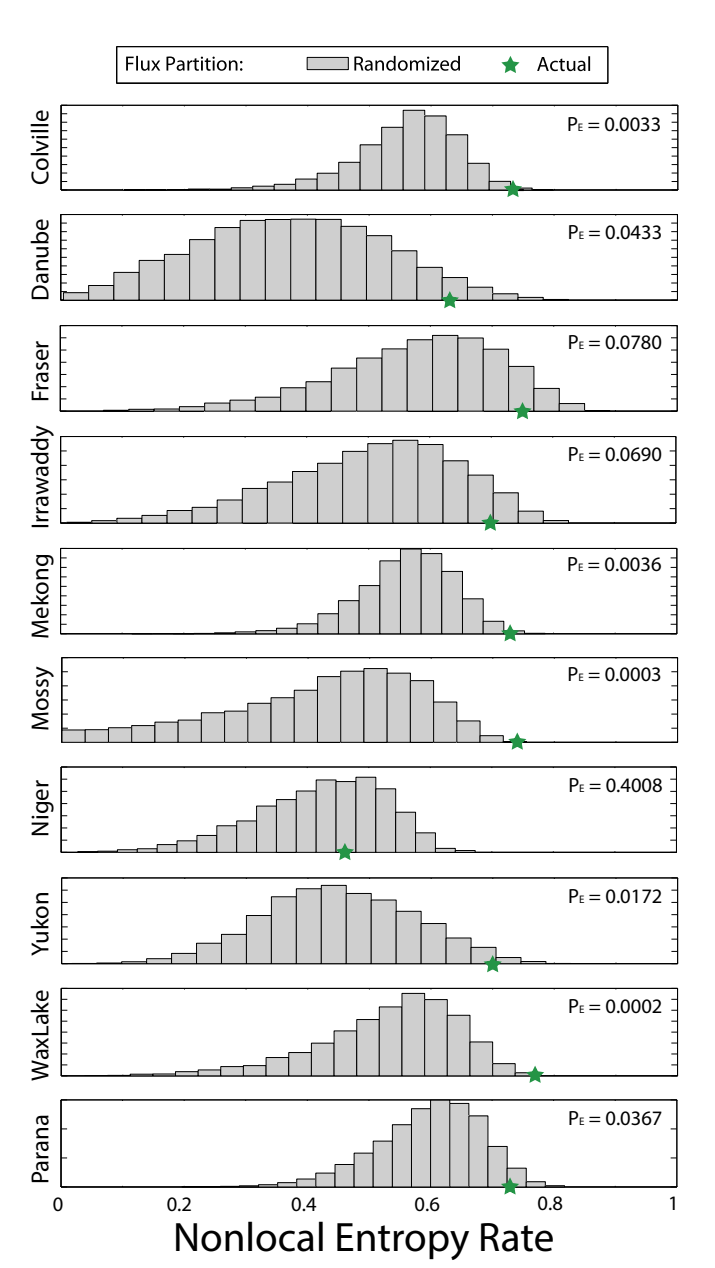


**Fig. 2.** nER for 10 field deltas. Green stars represent the values of nER computed for each field delta, using channel width (extracted from Landsat) as proxy for flux partition in bifurcations. We compared the values of nER for each delta with  $10^5$  randomizations of flux partitions (histograms). Nine out of the 10 deltas analyzed exhibit a maximal value of nER, defining maximal as a value where the probability of exceedance,  $P_E$ , by a random realization is less than 0.1.

47, 48) using the physically based hydromorphodynamic model Delft3D (see *SI Appendix* for further details). The results show that five of the six numerical deltas exhibit extreme values of nER with probability of exceedance  $P_E < 0.1$  (Fig. 3), further supporting our optimality hypothesis. Note that the simulated delta  $(D_{50} = 0.01 \text{ mm})$  that does not satisfy the optimality of nER is an extreme case, in terms of cohesiveness, for field deltas. Very cohesive banks are harder to erode and form levee breaches infrequently, delaying the triggering mechanism of avulsions. As a result, the system maintains itself at states at which the fluxes are not at equilibrium with its underlying channel network topology. This is reflected in suboptimal states of flux distribution and thus nER.

Tejedor et al. PNAS Early Edition | 3 of 6

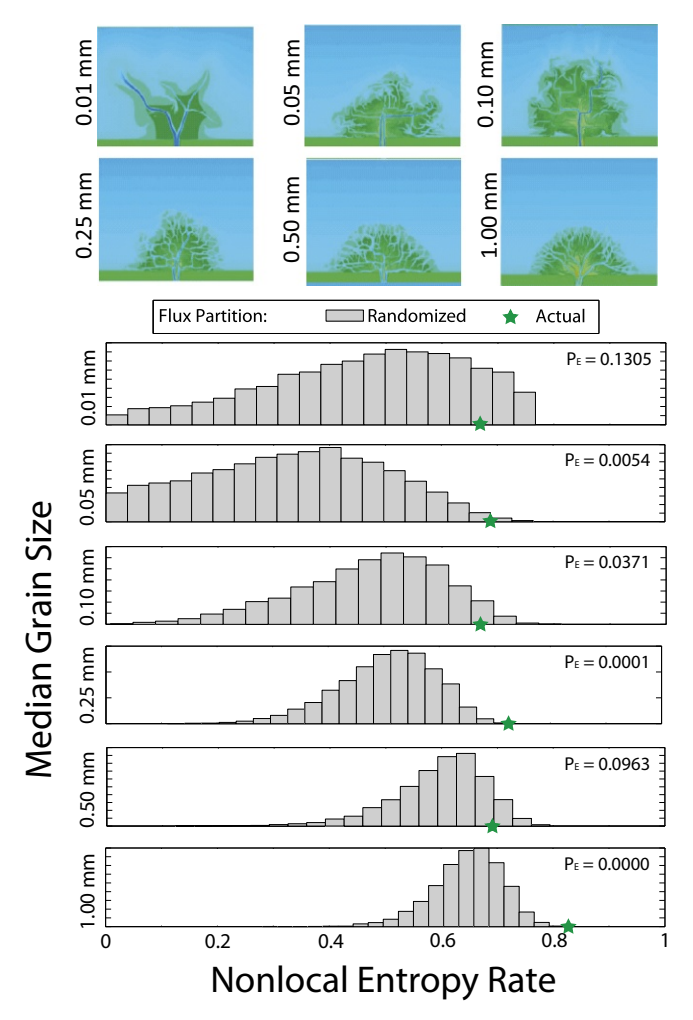


**Fig. 3.** nER for simulated deltas. We examine the nER of numerically simulated deltas obtained by the Delft3D model. The simulated deltas are riverdominated, with no vegetation, and with a lognormal distribution of incoming sediment size with median grain size  $D_{50}$  varying from 0.01 to 1.0 mm and the same variance in the log space (for more details see SI Appendix). These deltas exhibit a wide variety of channel network topologies as shown in ref. 32. Similar to the analysis conducted for the field deltas, green stars represent the values of nER using channel width (extracted from simulations) as proxy for flux partition in each bifurcation. Compared with  $10^5$  randomizations of flux partition (histogram), five out of six deltas analyzed exhibit a maximal value of nER, defining maximal as a value where the probability of exceedance by a random realization is less than 0.1.

Our results suggest that the flux partitions at each bifurcation, which have evolved naturally, are not random but rather follow a rule that optimizes the delta system as a whole. In fact, an interesting paradox arises from our analysis. Although the entropy introduced locally by each bifurcation, considered as an insulated unit, is suboptimal [the maximum would correspond to a symmetric bifurcation which is not consistent with stability theory of delta bifurcations that requires asymmetric local flux partition (45)], the specific assemblage of those bifurcations forming the delta network as a system is optimal (in terms of nER) and consistent with maximization of the diversity of fluxes delivered to the shoreline.

Turning attention to delta dynamics, we further hypothesize that during an avulsion the delta *nER* would decrease (see schematic in Fig. 4A). This is because during this phase of topologic reorganization the flux distribution inherited from the previous channel network structure is in general suboptimal with

respect to the incipient channel network reworked by the avulsion (i.e., the new channel structure created during the avulsion received a disproportionally small share of the flux, creating an asymmetry in the flux delivery to the shoreline and thus reducing the value of nER). Testing this hypothesis in field deltas is challenging because avulsions occur infrequently. However, using numerical models we can observe that during an avulsion cycle the nER drops significantly at the onset of a new flow path and following the abandonment of the old channel (Fig. 4B). Since the time scale of the avulsion itself is negligible in comparison with the lifespan of the topologies before and following the avulsion, it is observed that the flux partition is able to self-organize to achieve a configuration that maximizes nER. This supports our assumption that the time scale of the flux reorganization is several orders of magnitude smaller than the characteristic time scale of topologic reorganization which is set by the time lapse between avulsion cycles.

An important implication of this optimality principle can be interpreted in terms of the resilience of deltas to withstand perturbations. Intuitively, if a perturbation (e.g., flux reduction) is applied to a delta during its high-nER state, the perturbation will be damped as it will spread through the diverse pathways connecting the delta top to the shoreline. However, if the same perturbation is applied to a delta in a low-nER state, the perturbation will be more confined to a localized part of the delta but will exert a more severe disturbance. As revealed by our analysis, river deltas operate in configurations characterized by high values of nER, supporting the idea that deltas self-organize to achieve resilient morphologies priming self-maintenance. As a word of caution, especially relevant in the current scenario where deltas are subjected to increasing anthropogenic stresses, this distributive mechanism that dampens the intensity of perturbations can also lead to delta-wide catastrophic disturbances and tipping points when those perturbations exceed certain thresholds.

### **Conclusions**

Deltas are highly productive regions supporting extensive agriculture and aquaculture and diverse ecosystems and containing natural resources such as hydrocarbon deposits. Climate change and human actions, both in the upstream basins and locally, act as stressors on these landscapes, calling for a thorough understanding of these complex systems and their response to perturbations. We examined the existence of an optimality principle that governs the self-organization of water and sediment fluxes on delta channel networks. Specifically, (i) we put forth the hypothesis that maximizing nER, which quantifies the diversity in flux delivery to the shoreline, is a selective criterion in the evolutionary dynamics of delta networks; (ii) we tested this hypothesis by analyzing 10 field deltas of diverse complexity, age, and environmental settings and showed that all but one, the Niger delta, exhibited maximum nER; (iii) we further supported the existence of an optimality principle by analysis of Delft3D simulated deltas; (iv) we showed that during major reorganization, such as avulsions, nER exhibits suboptimal values and increases back to high rates (maximum values) when the flux distribution self-adjusts to the new delta channel network topology; and, finally, (v) we discussed the relation between entropy and resilience, arguing that delta flux configurations characterized by maximal nER are more resilient in the face of random perturbations. In the anthropocene where human activities have become a major agent of geomorphic change, understanding delta selforganization within an optimality perspective offers new ways of thinking about delta dynamics and disturbances that might hinder self-maintenance.

### **Materials and Methods**

**Deltas as Directed Graphs.** Tejedor et al. (29, 30) presented a rigorous framework based on graph theory within which a delta channel network is

represented by a directed graph, that is, a collection of vertices (bifurcations and junctions) and directed edges (channels in-between vertices, where the direction is given by the flow). All information about network connectivity and directionality of the flow can be stored in a sparse matrix called the adjacency matrix, A. Specifically, A is an  $N \times N$  matrix, where N is the number of vertices, and whose entry  $a_{ii}$  is unity if vertex i receives fluxes directly from vertex j (i.e., vertices i and j are connected by a link directed from j to i) and zero otherwise. From A we can derive an important matrix called Laplacian, which is equivalent to a diffusivity operator in a graph. To construct the Laplacian we need first to introduce the degree matrices for directed graphs. The in-degree (out-degree) matrix  $D^{in}$  ( $D^{out}$ ) is an  $N \times N$  diagonal matrix whose entries  $d_{ii}$  depict the number of links entering (exiting) vertex i and are computed as the sum of the entries in the i-th row (column) of A. The Laplacian matrix,  $L^{in}$  ( $L^{out}$ ), is defined as  $D^{in} - A$  ( $D^{out} - A$ ). Tejedor et al. (29, 30) showed that certain eigenvectors of the Laplacian operator contain important topologic information of the deltaic network. Furthermore, information about flux propagation can be obtained if A is replaced with the weighted adjacency matrix W, where the weights  $w_{ii}$  correspond to the fraction of flux in link (ji) with respect to the flux in vertex j. Similar to the at-station hydraulic geometry relationship (49)—width to landscapeforming discharge—reported for tributary rivers (50) and tidal channels (51), we assume the flux partition at the bifurcation to be proportional to the width of the downstream channels (18). Note that even though we do not consider explicitly in the computation of steady-state fluxes relevant processes such as water-sediment interchange between channel and islands (31, 52, 53), vegetation (54), tides (35), and so on, all of these processes set the hydrogeomorphic attributes of the channel network. Therefore, the computation of steady-state fluxes in the channel network based on physical attributes such as channel widths can be interpreted to a certain degree as the result of the integrative effect of all of the main processes acting on a delta. For the purposes of this paper, there are two probability distributions that can be computed by simple algebraic manipulation in the above-mentioned operators, namely, the steady-state flux distribution and the node-to-outlet transition probability distribution.

Steady-State Flux Distribution. Having a delta represented as a directed acyclic graph (DAG) allows us to compute the steady-state flux by assuming conservation of mass. For instance, Tejedor et al. (29) showed how the steady-state flux can be formulated as an eigenvalue–eigenvector problem of the Laplacian matrix of the graph. Here, we present the input/output model as a more intuitive way to compute the delta steady-state flux. Let us consider a DAG fed from the most upstream node (apex) with a constant unit flux. Without loss of generality, and for simplicity in the subsequent derivations, the apex is assumed to be labeled as node 1. Then, we can define the stationary distribution, F, as

$$F = \begin{pmatrix} 1 \\ 0 \\ 0 \\ \vdots \\ 0 \end{pmatrix} + W \begin{pmatrix} 1 \\ 0 \\ 0 \\ \vdots \\ 0 \end{pmatrix} + W^2 \begin{pmatrix} 1 \\ 0 \\ 0 \\ \vdots \\ 0 \end{pmatrix} + \dots = (I - W)^{-1} \begin{pmatrix} 1 \\ 0 \\ 0 \\ \vdots \\ 0 \end{pmatrix}, \qquad [4]$$

where the column vector  $\mathbf{e}_1 = (1\ 0\ 0\ \cdots\ 0)^T$  corresponds to the initial state, and W corresponds to the weighted adjacency matrix of the graph. Alternatively,  $\mathbf{e}_1$  represents a constant inflow at the apex normalized to 1, and  $W^k\mathbf{e}_1$  the resulting downstream response at time/distance specified by k. For a DAG, there exists at least one indexing of the graph such that each offspring vertex has a higher index than its parent vertex. In this indexing, by construction, the matrix W is strictly upper triangular, and therefore the matrix W is nilpotent, guaranteeing the convergence of the sum as expressed in Eq. 4. In SI Appendix we prove that the stationary flux distribution F can also be obtained as the stationary probability of a Markov process  $\pi$ .

**Node–Outlet Transition Probability Distribution.** The node-to-outlet transition probability,  $p_{ik}$ , is defined as the probability that a package of flux at node i drains to outlet k. Thus, the transport from each node i, to the different outlets M, can be understood as a discrete stochastic process with probability distribution  $\{p_{ik}\}$ , with k=1,...,M. Tejedor et al. (29) showed that when a delta channel network is represented by a directed acyclic graph G with a weighted adjacency matrix W,

i) The null space of the weighted in-degree Laplacian  $L_W^{in}(G^R)$  for the reverse graph  $G^R$  has dimension (multiplicity of the eigenvalue zero) equal to the number of outlets M;

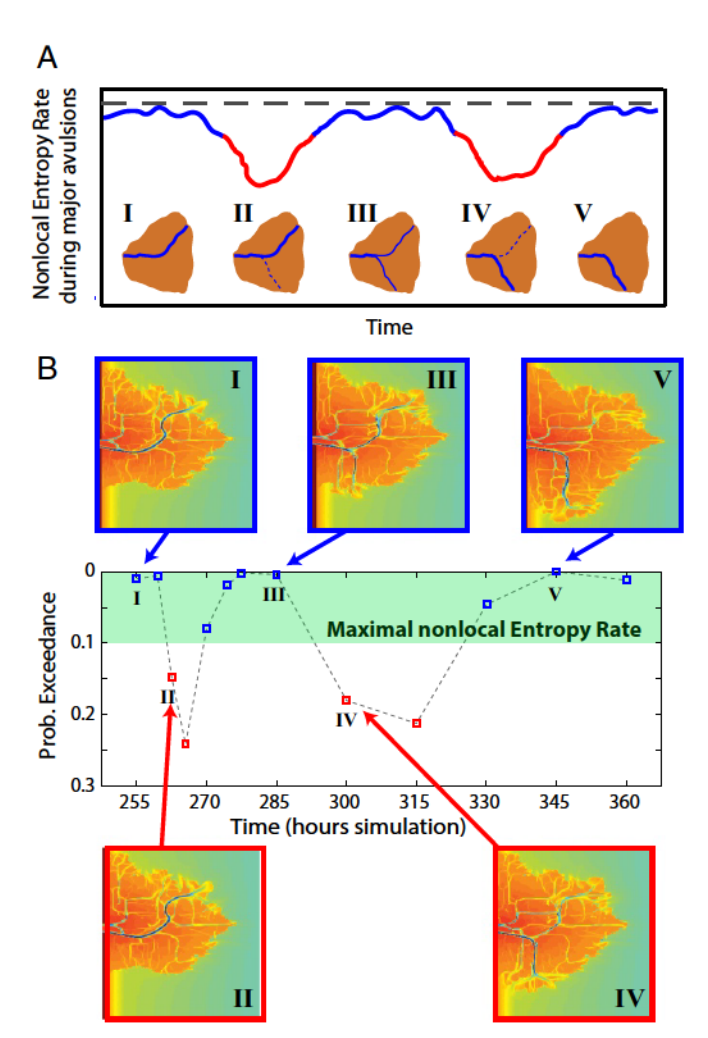


Fig. 4. nER during an avulsion cycle. (A) The results presented in Figs. 2 and 3 support the hypothesis that river deltas self-organize to maximize nER. However, deltas in dynamic equilibrium experience avulsions, periodically causing major reorganization of their channel networks. Our hypothesis is that during these periods of major reorganization delta nER drops significantly until the delta fluxes are self-organized back to a new structure as shown in the schematic of A. (Insets, from left to right) Schematics of the five stages within a single avulsion cycle (notice that for illustration purposes, only the main channel was drawn to better depict the avulsion cycle): (I) starting from a given channel network topology, (II) a new channel structure is created downstream of the avulsion node draining initially a small part of the flux, but progressively receiving larger proportions of fluxes until (III) the new and the old channel structures receive similar amounts of flux, and eventually transition to (IV) a configuration wherein the new channel structure has more flux, to finally lead to (V) the abandonment of the former channel structure downstream of the avulsion node. (B) We have tested this hypothesis using Delft3D simulations and analyzing subsequent instances of a delta evolution, wherein an avulsion cycle is observed. The probability (Prob.) of exceedance of the delta nER by a randomization of the flux configuration is displayed. The results agree with the posed hypothesis, showing that nER drops at the beginning and end of the avulsion cycle, keeping a maximal value otherwise.

ii) There exists a unique basis  $\gamma_k$ ,  $k=1,\cdots,M$ , of this null space in  $\mathbb{R}^N$  (i.e., the basis consists of M vectors each having N entries) with the property

$$\gamma_k(i) = \begin{cases} 1, & i = k \\ 0, & i \neq k \end{cases} \text{ for } k = 1, \dots, M.$$
 [5]

Tejedor et al. PNAS Early Edition | 5 of 6

That is, the entry of the vector  $\gamma_k$  corresponding to outlet k is one, and zero at all other outlets.

iii) The value  $\gamma_k(i)$  represents the portion of flux at the vertex i that drains to the outlet k, that is,  $p_{ik}$ .

Thus, if we define a matrix T, whose columns form the basis of the null space of  $L_W^{in}(G^R)$ ,  $\{\gamma\}$ , then the *i*-th row corresponds to the probability distribution  $\{p_{ik}\}$ .

- 1. Cohen J, Small C, Mellinger A, Gallup J, Sachs J (1997) Estimates of coastal populations. Science 278:1209-1213.
- 2. Ericson J, Vörösmarty C, Dingman S, Ward L, Meybeck M (2006) Effective sea-level rise and deltas: Causes of change and human dimension implications. Glob Planet Change 50:63-82.
- 3. Woodroffe C, Nicholls R, Saito Y, Chen Z, Goodbred S (2006) Landscape Variability and the Response of Asian Megadeltas to Environmental Change, ed Harvey N (Springer, Dordrecht, The Netherlands), pp 277-314.
- Syvitski J, et al. (2009) Sinking deltas due to human activities. Nat Geosci 2:681–686.
- Vörösmarty C, et al. (2009) Battling to save the world's river deltas. Bull At Sci 65: 31-43
- 6. Hoanh C, Szuster B, Suan-Pheng K, Ismail A, Noble A, eds (2010) Tropical Deltas and Coastal Zones: Food Production, Communities and Environment at the Land-Water Interface (CAB, Wallingford, UK), p 496.
- Barbier E, et al. (2011) The value of estuarine and coastal ecosystem services. Ecol Monogr 81:169-193.
- Foufoula-Georgiou E, et al. (2013) A Vision for a Coordinated International Effort on Delta Sustainability, eds Young G, Perillo G (IAHS, Gothenburg, Sweden), pp 3-11.
- 9. Brondizio E, et al. (2016) Catalyzing action towards the sustainability of deltas. Curr Opin Environ Sustain 19:182-194.
- 10. Szabo S, et al. (2016) Population dynamics, delta vulnerability and environmental change: Comparison of the Mekong, Ganges-Brahmaputra and Amazon delta regions. Sustain Sci 11:539-554.
- 11. Syvitski J, Vörösmarty C, Kettner A, Green P (2005) Impact of humans on the flux of terrestrial sediment to the global coastal ocean. Science 308:376-380.
- 12. Blum M. Roberts H (2009) Drowning of the Mississippi delta due to insufficient sediment supply and global sea-level rise. Nat Geosci 2:488-491.
- 13. Kirwan M, Megonigal J (2013) Tidal wetland stability in the face of human impacts and sea-level rise. Nature 504:53-60.
- 14. Giosan L, Syvitski J, Constantinescu S, Day J (2014) Climate change: Protect the world's deltas. Nature 516:31-33.
- 15. Tessler Z, et al. (2015) Profiling risk and sustainability in coastal deltas of the world. Science 349:638–643.
- 16. Wang S, et al. (2015) Reduced sediment transport in the yellow river due to anthropogenic changes. Nat Geosci 9:38-41.
- Sebesvari Z, et al. (2016) A review of vulnerability indicators for deltaic socialecological systems. Sustain Sci 11:575–590.
- 18. Edmonds D, Paola C, Hoyal D, Sheets B (2011) Quantitative metrics that describe river deltas and their channel networks. J Geophys Res 116:2156-2202.
- 19. Rodriguez-Iturbe I, Rinaldo A (2001) Fractal River Basins: Chance and Self-Organization (Cambridge Univ Press, New York), 2nd Ed, p 547.
- 20. Banavar J, Maritan A, Rinaldo A (2000) Topology of the fittest network. Phys Rev Lett 84:4745-4748.
- 21. Banavar J, Colaiori F, Flammini A, Maritan A, Rinaldo A (2001) Scaling, optimality, and landscape evolution. J Stat Phys 104:1-48.
- 22. Rinaldo A, Rigon R, Banavar J, Maritan A, Rodriguez-Iturbe I (2014) Evolution and selection of river networks: Statics, dynamics, and complexity. Proc Natl Acad Sci USA 111-2417-2424
- 23. West G, Brown J, Enquist B (1997) A general model for the origin of allometric scaling laws in biology. Science 276:122-126.
- 24. West G, Brown J, Enquist B (1999) A general model for the structure and allometry of plant vascular systems. Nature 400:664–667
- 25. Hildebrandt A, Kleidon A, Bechmann M (2016) A thermodynamic formulation of root water uptake. Hydrol Earth Syst Sci Discuss 20:3441-3454.
- 26. Kleidon A, Renner M, Porada P (2014) Estimates of the climatological land surface energy and water balance derived from maximum convective power. Hydrol Earth Syst Sci Discuss 18:2201-2218.
- 27. Kleidon A, Kravitz B, Renner M (2015) The hydrological sensitivity to global warming and solar geoengineering derived from thermodynamic constraints. Geophys Res Lett 42:138-144.
- 28. Dhara C, Renner M, Kleidon A (2016) Broad climatological variation of surface energy balance partitioning across land and ocean predicted from the maximum power limit. Geophys Res Lett 43:7686-7693.

ACKNOWLEDGMENTS. This work is part of the International BF-DELTAS project on "Catalyzing action toward sustainability of deltaic systems" funded by the Belmont Forum (NSF Grant EAR-1342944) and the Linked Institutions for Future Earth (NSF Grant EAR-1242458). This work was partially supported by the FESD Delta Dynamics Collaboratory (NSF Grant EAR-1135427), the Water Sustainability and Climate Program (NSF Grant EAR-1209402), and NSF Grant ECCS-1509387. A.T. acknowledges financial support from a National Center for Earth-surface Dynamics 2 postdoctoral fellowship (NSF Grant EAR-1246761).

- 29. Tejedor A, Longjas A, Zaliapin I, Foufoula-Georgiou E (2015) Delta channel networks: 1. A graph-theoretic approach for studying connectivity and steady state transport on deltaic surfaces. Water Resour Res 51:3998-4018.
- 30. Tejedor A, Longjas A, Zaliapin I, Foufoula-Georgiou E (2015) Delta channel networks: 2. Metrics of topologic and dynamic complexity for delta comparison, physical inference, and vulnerability assessment. Water Resour Res 51:4019-4045.
- 31. Hiatt M, Passalacqua P (2015) Hydrological connectivity in river deltas: The first-order importance of channel-island exchange. Water Resour Res 51:2264-2282.
- 32. Tejedor A, et al. (2016) Quantifying the signature of sediment composition on the topologic and dynamic complexity of river deltas. Geophys Res Lett 43:3280-
- 33. Liang M, Van Dyk C, Passalacqua P (2016) Quantifying the patterns and dynamics of river deltas under conditions of steady forcing and relative sea level rise. J Geophys Res Earth Surf 121:465-496.
- 34. Passalacqua P (2017) The delta connectome: A network-based framework for studying connectivity in river deltas. Geomorphology 277:50-62.
- 35. Fagherazzi S (2008) Self-organization of tidal deltas. Proc Natl Acad Sci USA 105:18692-18695.
- 36. Chatanantavet P, Lamb M, Nittrouer J (2012) Backwater controls of avulsion location on deltas. Geophys Res Lett 39:L01402.
- 37. Ganti V, Chu Z, Lamb M, Nittrouer J, Parker G (2014) Testing morphodynamic controls on the location and frequency of river avulsions on fans versus deltas: Huanghe (Yellow river), China. Geophys Res Lett 41:7882-7890.
- 38. Shannon C (1948) A mathematical theory of communication. Bell Syst Tech J 27:379-423, 623-656.
- 39. Jaynes E (1957) Information theory and statistical mechanics. Phys Rev 106:620-630.
- 40. Dewar R (2003) Information theory explanation of the fluctuation theorem, maximum entropy production and self-organized criticality in non-equilibrium stationary states. J Phys A Math Gen 36:631-641.
- 41. Martyushev L, Seleznev V (2006) Maximum entropy production principle in physics, chemistry and biology. Phys Rep 426:1-45.
- 42. Cover T, Thomas J (2006) Elements of Information Theory (Wiley, Hoboken, NJ), 2nd Ed, p 748.
- 43. Slingerland R, Smith N (2004) River avulsions and their deposits. Annu Rev Earth Pl Sc
- 44. Ganti V, Chadwick A, Hassenruck-Gudipati H, Lamb M (2016) Avulsion cycles and their stratigraphic signature on an experimental back-water-controlled delta. J Geophys Res Earth Surf 121:1651-1675.
- 45. Edmonds D, Slingerland R (2008) Stability of delta distributary networks and their bifurcations. Water Resour Res 44:W09426.
- 46. Bolla Pittaluga M, Coco G, Kleinhans M (2015) A unified framework for stability of channel bifurcations in gravel and sand fluvial systems. Geophys Res Lett 42:7521-7536
- 47. Edmonds D, Slingerland R (2010) Significant effect of sediment cohesion on delta morphology. Nat Geosci 3:105-109.
- 48. Caldwell R, Edmonds D (2014) The effects of sediment properties on deltaic processes and morphologies: A numerical modeling study. J Geophys Res Earth Surf 119:961-
- 49. Leopold L, Maddock T, Jr. (1953) The hydraulic geometry of stream channels and some physiographic implications. US Geol Surv Prof Pap 252:1–52.
- Dodov B, Foufoula-Georgiou E (2004) Generalized hydraulic geometry: Derivation based on a multiscaling formalism. Water Resour Res 40:W06302.
- 51. Rinaldo A, Fagherazzi S, Lanzoni S, Marani M, Dietrich W (1999) Tidal networks: 2. Watershed delineation and comparative network morphology. Water Resour Res 35:3905-3917.
- 52. Shaw J, Mohrig D, Wagner R (2016) Flow patterns and morphology of a prograding river delta. J Geophys Res Earth Surf 121:372-391.
- 53. Wagner W, et al. (2017) Elevation change and stability on a prograding delta. Geophys Res Lett 44:1786-1794.
- 54. Nardin W, Edmonds DA (2014) Optimum vegetation height and density for inorganic sedimentation in deltaic marshes. Nat Geosci 7:722-726.

# Supporting Information (SI Appendix)

## Entropy and optimality in river deltas

Alejandro Tejedor<sup>a</sup>, Anthony Longjas<sup>a</sup>, Douglas A. Edmonds<sup>b,c</sup>, Ilya Zaliapin<sup>d</sup>, Tryphon T. Georgiou<sup>e</sup>, Andrea Rinaldo<sup>f,g</sup>, and Efi Foufoula-Georgiou<sup>a</sup>

<sup>a</sup> Department of Civil and Environmental Engineering, University of California, 92697 Irvine, California, USA; <sup>b</sup> Department of Earth and Atmospheric Sciences, Indiana University, Bloomington, IN 47405; <sup>c</sup> Center for Geospatial Data Analysis, Indiana University, Bloomington, IN 47405; <sup>d</sup> Department of Mathematics and Statistics, University of Nevada, Reno, Nevada, USA; <sup>e</sup> Department of Mechanical and Aerospace Engineering, University of California, 92697 Irvine, California, USA; <sup>f</sup> Laboratory of Ecohydrology, Ecole Polytechnique Federale Lausanne, 1015 Lausanne, Switzerland; <sup>g</sup> Dipartimento di Ingegneria Civile, Edile ed Ambientale, Universitá di Padova, 35131 Padova, Italy

# Equivalence of the Input/output model to a Markov process

In this section, we prove the equivalence of the stationary probabilities that result from an irreducible and aperiodic discrete Markov process and the input/output model introduced in the Materials and Methods section.

Irreducible and aperiodic discrete Markov process. Let P be the transition probability matrix of a discrete Markov process which is irreducible (all the states are reachable from any state) and aperiodic (the return period to a given state can occur at different time steps),

$$P = \left\{ p_{ij} \right\}_{NxN} . \tag{1}$$

P is an  $N \times N$  square matrix, being N the number of states, and  $p_{ij}$  the probability of transition from state j to state i at each time step. Then, we can define a stationary probability distribution  $\pi$ :

$$P\pi = \pi, [2]$$

where  $\pi = {\pi_i}_{Nx_1}$  is a column vector, whose entries correspond to the stationary probability distribution of each state *i*. Therefore,  $\pi_i$  are non-negative values, satisfying  $\sum_{i=1}^{N} \pi_i = 1$ .

For a given directed acyclic graph, such as the ones we used to represent delta channel networks, if we assume conservation of mass, the dynamics of the system can be modelled by a Markov process where the outlets of the graph are reconnected to the apex with transition probability one. Thus, the transition probability matrix is equal to the weighted adjacency matrix of the graph, W, if the entries  $w_{ij}$  corresponding to transition outlets to the apex are substituted by ones.

Equivalence of the Input/output model and Markov process solutions. We have shown in the Materials and Methods section that for a delta conceptualized as a directed acyclic graph fed from the most upstream node (apex) with a constant unit flux, we can compute the steady-state flux distribution F as:

$$F = (I - W)^{-1} \begin{pmatrix} 1 \\ 0 \\ 0 \\ \vdots \\ 0 \end{pmatrix}.$$
 [3]

We prove in this section that the stationary distributions obtained from an irreducible and aperiodic Markov process,  $\pi$ , and an input/output model, F, are equivalent (up to a normalization factor). To prove this statement, we can decompose

the transition probability matrix of the Markov process P as  $P=W+R,\ R$  is called the recirculation matrix and it is defined as follows:

$$R = \left\{ r_{ij} = \delta_{i1} \delta_{j\{k\}} \right\}_{N_T N}.$$
 [4]

where  $\delta$  represents the Kronecker delta; and therefore, all the entries of matrix R are zeros, except for the entries of the first row (apex has been indexed with i=1 without loss of generality) that correspond to  $\{k\}$ -columns indexing the outlets.

*Proof.* If  $F=\pi$ , then F must be an eigenvector of the probability transition matrix P, and therefore PF=F. Given,

$$\begin{cases}
F = (I - W)^{-1} \begin{pmatrix} 1 \\ 0 \\ 0 \\ \vdots \\ 0 \end{pmatrix} \\
P = W + R
\end{cases} [5]$$

then,

$$(W+R)(I-W)^{-1} \begin{pmatrix} 1\\0\\0\\\vdots\\0 \end{pmatrix} = (I-W)^{-1} \begin{pmatrix} 1\\0\\0\\\vdots\\0 \end{pmatrix}.$$
 [6]

By multiplying both sides of Eq. 6 from the left by (I - W),

$$(I - W)(W + R)(I - W)^{-1} \begin{pmatrix} 1 \\ 0 \\ 0 \\ \vdots \\ 0 \end{pmatrix} = \begin{pmatrix} 1 \\ 0 \\ 0 \\ \vdots \\ 0 \end{pmatrix}.$$
 [7]

Expanding the left side of Eq. 7,

$$(I-W)W(I-W)^{-1} \begin{pmatrix} 1\\0\\0\\\vdots\\0 \end{pmatrix} + (I-W)R(I-W)^{-1} \begin{pmatrix} 1\\0\\0\\\vdots\\0 \end{pmatrix} = \begin{pmatrix} 1\\0\\0\\\vdots\\0 \end{pmatrix}.$$
[8]

Simplifying and rearranging Eq. 8,

$$W\begin{pmatrix} 1\\0\\0\\\vdots\\0 \end{pmatrix} + (I - W)R(I - W)^{-1}\begin{pmatrix} 1\\0\\0\\\vdots\\0 \end{pmatrix} = \begin{pmatrix} 1\\0\\0\\\vdots\\0 \end{pmatrix}, \quad [9]$$

$$(I - W)R(I - W)^{-1} \begin{pmatrix} 1 \\ 0 \\ 0 \\ \vdots \\ 0 \end{pmatrix} = (I - W) \begin{pmatrix} 1 \\ 0 \\ 0 \\ \vdots \\ 0 \end{pmatrix}, \quad [10]$$

$$R(I - W)^{-1} \begin{pmatrix} 1 \\ 0 \\ 0 \\ \vdots \\ 0 \end{pmatrix} = \begin{pmatrix} 1 \\ 0 \\ 0 \\ \vdots \\ 0 \end{pmatrix}.$$
 [11]

Defining  $B = R(I - W)^{-1}$ ,

$$B \begin{pmatrix} 1 \\ 0 \\ 0 \\ \vdots \\ 0 \end{pmatrix} = \begin{pmatrix} 1 \\ 0 \\ 0 \\ \vdots \\ 0 \end{pmatrix}.$$
 [12]

Considering the structure of matrix R (see Eq. 4), then B is also a sparse matrix with the following entries:

$$B = \left\{b_{ij}\right\}_{NxN}; b_{ij} = \sum_{l=1}^{N} r_{il} (I - W)_{lj}^{-1} \delta_{1i} \delta_{l\{k\}}, \quad [13]$$

where the only non-zeros entries of the B matrix are in the first row (the apex has been indexed with i = 1 without loss of generality). Thus, the condition needed to satisfy Eq. 13 is simply that the entry  $b_{11} = 1$ . Therefore,

$$b_{11} = \sum_{l=1}^{N} r_{1l} (I - W)_{l1}^{-1} \delta_{l\{k\}} = \sum_{l=1}^{N} (I - W)_{l1}^{-1} \delta_{l\{k\}} = 1. [14]$$

In other words, the sum of the entries of the first column of  $(I-W)^{-1}$  that corresponds to the outlets,  $\{k\}$ , must be equal to one.

Given the definition of the input/output model (see Eq. 3), the first column of  $(I-W)^{-1}$  stores the values of the fluxes, F. Assuming conservation of mass, and that the input of the model is set to 1, the sum of the fluxes of the outlets must be one also, proving that the Markov model based on the idea of recirculating the flux and Input/Ouput model provide consistent stationary probability distributions.

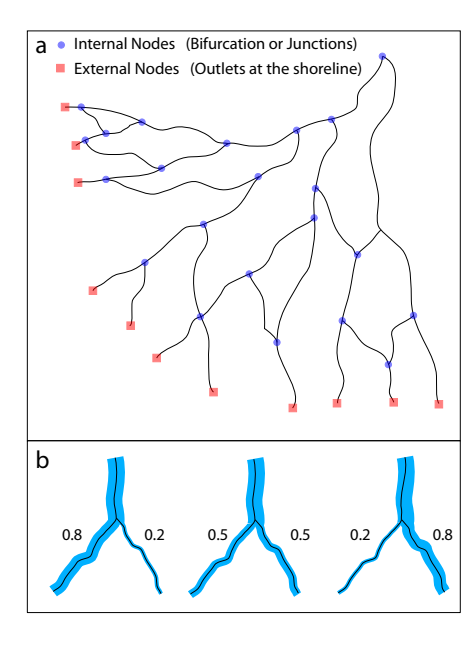


**Fig. 1.** Graph representation of a delta and nonlocal Entropy Rate (nER) for deltas. (a) A river delta channel network topology can be represented by a graph where channels correspond to links in the graph, and junctions and bifurcations are internal nodes (blue circles). Delta outlets are represented as external nodes (red squares). The graphs used in this paper to model delta channel networks are directed graphs (link direction corresponds to the direction of the flow in the channel) and acyclic (no cycles, i.e., water recirculation). All the information in the graph can be stored in a sparse matrix called Adjacency matrix (see text in Tejedor et al. (1) and supporting information for further details). (b) The topologic representation of a delta channel network does not contain any relevant information (besides flux directionality) about flux dynamics, and more specifically about flux partition in the bifurcations. Thus, for the same topologic configuration, such a bifurcation can exhibit very different flux partition depending on its physical attributes. Here, we use downstream channel width as a proxy of the flux partition in bifurcations. This graph representation allows us to compute algebraically different properties of the graph, including the stationary flux distribution when a constant flow input is supplied through the delta apex. One of the magnitudes that we can compute is what we define as nER. Intuitively, nERcan be understood as the average amount of information (or uncertainty) needed to track packages of flux in their journey from an internal node (blue circle in a) to the outlet (red square) where it is delivered. We hypothesized that nER is maximized by delta self-organization, adjusting flux partition to maximize this uncertainty metric. To test this hypothesis, we compare the value of nER computed using channel width as proxy for flux partition, with values of nER computed when the flux partition in each bifurcation is randomized, i.e., the channel network structure (topology) is preserved but the flux partition changes at the bifurcation scale as is exemplified in b.

### Physical characteristics of the ten deltas analyzed

In this section, we summarize the physical characteristics of the ten deltas selected for analysis namely: Niger, Parana, Yukon, Irrawaddy, Colville, Wax Lake, Mossy, Fraser, Danube and Mekong (Fig. 2). Extracting the channel networks from an air photo or satellite image of a delta is not an easy task. For this reason, we have adopted here for our preliminary analysis the exact five traced deltas in the study of Smart and Moruzzi (2) – Niger, Parana, Yukon, Irrawaddy, and Colville – and have added the Wax Lake and Mossy deltas for which channel networks have been extracted in previous studies (3). We also added the channel networks of Fraser, Danube and Mekong extracted from Google Earth satellite images.

Niger Delta: The Niger delta is located in the West coast of Nigeria (latitude  $4.95^{\circ}$ , longitude  $6.18^{\circ}$ ). It receives input from the Niger River with an average water discharge of 6,130 m<sup>3</sup>s<sup>-1</sup> and sediment discharge of  $3.97 \times 10^{7}$  tons yr<sup>-1</sup> (4).

2 | Tejedor et al.

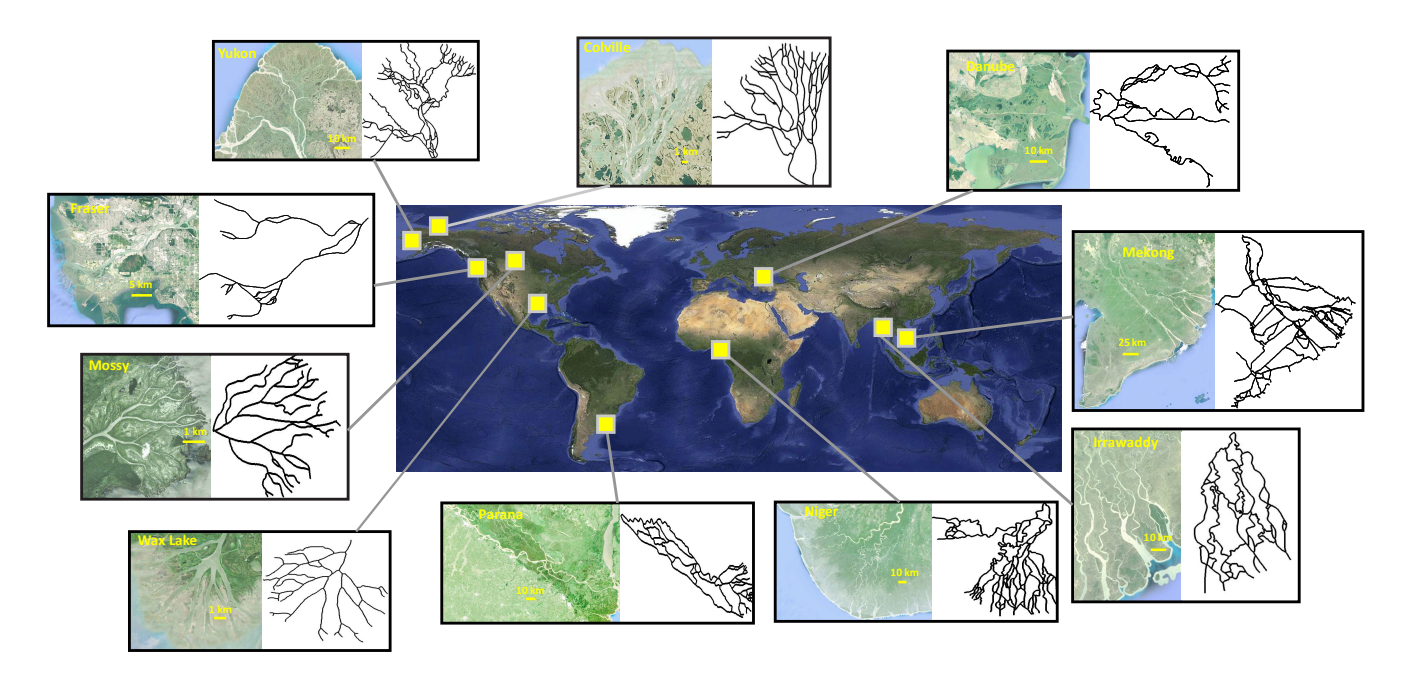


Fig. 2. Field deltas and their channel network structure. Clockwise starting from top left: Yukon, Colville, Danube, Mekong, Irrawaddy, Niger, Parana, Wax Lake, Mossy, and Fraser. Satellite images provided by Landsat/Copernicus, NASA, Digital Globe and CNES/Airbus were extracted from Google Earth. We acknowledge their respective copyrights.

Niger delta is the largest delta in Africa covering an area of 24,508 km<sup>2</sup>, sediment is mostly fine sand (5) and the tidal range is 3.0 m. The origin of the delta is estimated to be 80 - 35 million years BP during the Late Cretaceous (6). It is classified as tide and wave dominated (4). By using the channel network extracted by Smart and Moruzzi (2), we identified 181 links, 130 vertices and 15 shoreline outlets.

Parana Delta: The Parana delta is located North of Buenos Aires, Argentina (-33.80°, -59.25°). It is fed by the Parana River, which delivers an average water discharge of 13,600  $\rm m^3 s^{-1}$  and sediment discharge of 7.75 x  $10^7$  tons  $\rm yr^{-1}$  (4). Parana delta covers an area of 15,463 km² and sediment are mostly fine sand, silt and clay (8), and the tidal range is 4.0 m. Delta genesis was estimated during the Middle Holocene (6,000 years BP) (7). It is classified as a river and geology dominated delta (4). By using the channel network extracted by Smart and Moruzzi (2), we identified 86 links, 69 vertices and 18 shoreline outlets.

Yukon Delta: The Yukon Delta, located in the West coast of Alaska, USA (63.05°, -164.05°) receives input from the Yukon River with an average water discharge of 6,620 m<sup>3</sup>s<sup>-1</sup> and sediment discharge of 5.97 x 10<sup>7</sup> tons yr<sup>-1</sup> (4). It has an area covering 8,313 km<sup>2</sup> with mainly fine-grained sediments (10) and the tidal range is 1.5 m. Delta genesis is estimated to be during the Middle Holocene (5,000 years BP) (9). It is classified as a wave dominated delta (4). By using the channel network extracted by Smart and Moruzzi (2), we identified 169 links, 126 vertices and 24 shoreline outlets in the delta.

Irrawaddy Delta: The Irrawaddy delta is located in the Southernmost coast of Myanmar ( $16.20^{\circ}$ ,  $95.00^{\circ}$ ). It is fed by the Irrawaddy River at an average water discharge of 13,558 m<sup>3</sup>s<sup>-1</sup> and sediment discharge of  $2.60 \times 10^{8}$  tons yr<sup>-1</sup> (4). The delta covers an area of 6,438 km<sup>2</sup> with the deposited sediment composed of mostly mixed mud and silt (5), and the tidal

range is 4.2 m. It is estimated that the delta began to form around 8,000-7,000 years BP together with most of the deltas in Southeast Asia (11). It is classified as a tide dominated delta (4). By using the channel network extracted by Smart and Moruzzi (2), we identified 100 links, 71 vertices and 6 shoreline outlets in the delta.

Colville Delta: The Colville delta, located in the Northern part of Alaska, USA  $(70.40^{\circ}, -150.65^{\circ})$ , receives input from the Colville River with an average water discharge of 491.7 m<sup>3</sup>s<sup>-1</sup> (5) and sediment discharge of 1.16 x 10<sup>8</sup> tons yr<sup>-1</sup> (12). With an area of 240 km<sup>2</sup>, it is relatively small compared to other polar deltas. Sediment is mostly composed of gravel and sand (5). The tidal range is 0.2 m. The delta began to develop during the Middle Holocene (4,000 years BP) (13). It is classified as a river dominated delta (4). By using the channel network extracted by Smart and Moruzzi (2), we identified 140 links, 107 vertices and 20 shoreline outlets in the delta.

Wax Lake Delta: The Wax Lake delta, located in the coast of Louisiana, USA  $(29.51^{\circ}, -91.44^{\circ})$ , receives input from the Wax Lake outlet, a channel that was dredged in the early 1940s to mitigate flooding risk in the nearby Morgan City, at an average water discharge of  $2.900 \,\mathrm{m^3 s^{-1}}$  and sediment discharge of  $2.35 \,\mathrm{x} \,10^7$  tons  $\mathrm{yr^{-1}}$  (14). The slope of the Wax Lake delta from the delta apex to the Gulf of Mexico is  $5.8 \,\mathrm{x} \,10^{-5}$  (15). Subaerial land only developed after the 1970s flood and has been experiencing rapid growth in the last two decades doubling to more than 100 km² today (16, 17). Sediment deposit in the delta is composed of approximately 67% sand (16), and the tidal range is 0.40 m (18). It is classified as a river dominated delta. We utilized the outline of the Wax Lake delta channel network processed by Edmonds et al. (3) containing 59 links, 56 vertices and 24 shoreline outlets.

Mossy Delta: The Mossy delta is located in Saskatchewan, Canada (54.07°, -102.35°). It is fed by the Mossy River with an average water discharge of 300 m³s<sup>-1</sup>(3) and sediment discharge of 2.20 x 10<sup>6</sup> tons yr<sup>-1</sup> (19). The delta was formed as a result of the avulsion of the Saskatchewan River in the 1870s (20). Progradation of the delta resulted in an area of 14 km² in the early 1940s (19) and after the construction of a spillway dam in the 1960s, the delta ever since slowly evolved with a current area of approximately 17 km². Sediment in the delta is roughly 50% fine-grained sand (3). Since the delta drains into a lake (Lake Cumberland), the effect of tides is insignificant. It is classified as a river dominated delta. We have extracted the channel network of Mossy delta and identified 67 links, 61 vertices and 23 shoreline outlets.

Danube Delta: The Danube delta is located in Romania  $(45.2^{\circ}, 29.4^{\circ})$  and receives input from the Danube River with an average water discharge of  $6,420~\mathrm{m}^3\mathrm{s}^{-1}$  and sediment discharge of  $6.72~\mathrm{x}~10^7$  tons  $\mathrm{yr}^{-1}$  (4). It has an area of  $6,468~\mathrm{km}^2$ . Main control of the delta is waves (southern part) although the northern part is river-dominated (21). Recent studies show that the intensification of land use in the watershed as the population increased and land use technology has increased sedimentation in the delta (22).

Fraser Delta: The Fraser delta is located in Canada (49.18°, -122.95°) and receives input from the Fraser River with an average water discharge of  $3,560~\rm m^3 s^{-1}$  and sediment discharge of  $2.00~\rm x~10^7$  tons yr $^{-1}$  (4). It has an area of  $876~\rm km^2$ . Main control of the delta is river and tide. Recent studies show that the delta is experiencing more human intervention.

Mekong Delta: The Mekong delta is located in Vietnam  $(10.1^{\circ}, 150.6^{\circ})$  and receives input from the Mekong River with an average water discharge of  $14,770 \text{ m}^3\text{s}^{-1}$  and sediment discharge of  $1.60 \times 10^7 \text{ tons yr}^{-1}$  (4). It has an area of  $91,789 \text{ km}^2$ . Main control of the delta is river and wave.

#### **Delft3D Numerical Simulations**

We use Delft3D to simulate the self-formed evolution of delta distributary networks. Delft3D is a physics-based morphodynamic model that has been validated for morphodynamics applications (23). We employ the depth-averaged version of Delft3D, which solves the unsteady shallow water equations in the horizontal dimension and assumes hydrostatic pressure in the vertical. Specifically, in this paper, we use model runs from Caldwell and Edmonds (24), which simulate a sediment-laden river entering a standing body of water that is devoid of waves, tides, and buoyancy forces. The river has an upstream water discharge boundary condition (steady flow of 1000 m<sup>3</sup>s<sup>-1</sup>) and carries sediment fluxes in equilibrium with the flow field. The downstream water surface boundary conditions are fixed at sea level. The flow field is coupled to the sediment transport equations (25, 26) and bed surface equations so it dynamically evolves in response to sediment transport gradients. The incoming sediment consists of grain sizes, D, lognormally distributed with a median size,  $D_{50}$ , and standard deviation  $\sigma(\phi)$ (in  $\phi$  space, where  $\phi = \log_2 D$ ). We note that cohesiveness (defined as the percent of sediment with grain size  $D < D_c$ = 0.064 mm) and dominant grain size  $(D_{84})$  can be uniquely determined as a function of  $D_{50}$  and  $\sigma(\phi)$  when the sediment size is lognormally distributed. Notice that other variables that can affect directly or indirectly the bulk cohesion of the system (e.g., vegetation, flow variability, and spatial hetero-

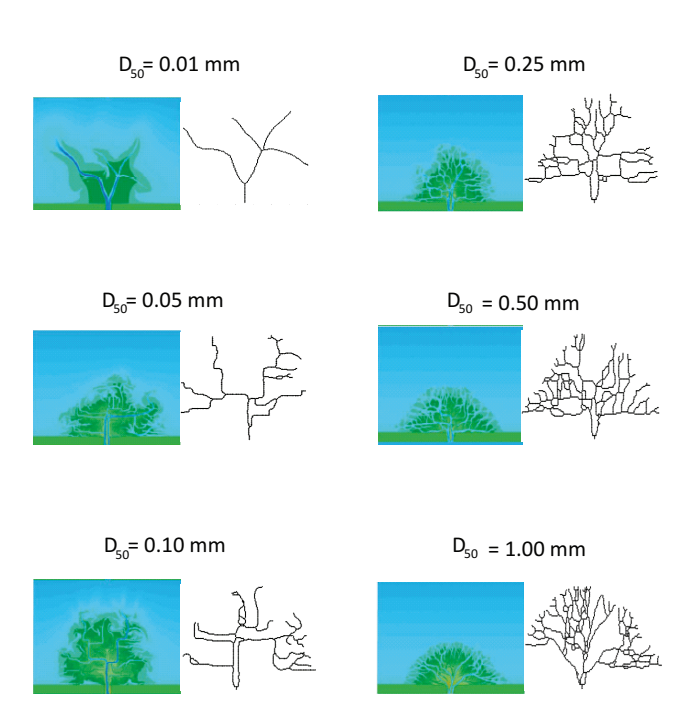


**Fig. 3.** Numerical deltas and their channel network structure. Six river dominated deltas (no wave or tidal energy) are displayed where the only difference is the median of the incoming grain size distributions  $D_{50}$  = 0.01 mm, 0.05 mm, 0.10 mm, 0.25 mm, 0.50 mm, and 1.00 mm.

geneities from apex to shoreline) have not been considered here. Specifically, we compare six runs where the only difference is the median of the incoming grain size distributions  $D_{50}$ , while the standard deviation is fixed to  $\sigma(\phi)=1$ . The distributions have median sizes of 0.01 mm, 0.05 mm, 0.1 mm, 0.25 mm, 0.5 mm, and 1 mm, respectively (Fig. 3). These simulations are identical to runs B1a1, B1c1, B1e1, B1h1, B1m1, and B1o1 in Table 2 of Caldwell and Edmonds (24), exploring the whole range of cohesiveness (from 0% to 100%) and values of dominant grain size from 0.014 to 1.896 mm. For more discussion on the morphodynamics of these deltaic simulations, see Caldwell and Edmonds (24).

We utilized the capability of numerical simulations to investigate the change in nER during an avulsion cycle. Fig. 4 shows the avulsion cycle analyzed in this paper obtained from the run with  $D_{50}=0.10$  mm.

Channel Network Extraction and Analysis. The analysis conducted in this paper relies on spectral graph theory, which requires transforming each delta channel network into a graph. Graphs are mathematical objects composed of vertices and edges. For delta channel networks, the edges represent channels, and vertices correspond to the locations where one channel splits into new channels (bifurcation) or two or more channels merge into a single channel (junction). In pre-processing the gridded data produced by the simulations, we perform the following steps:

 Classify pixels as Land/Channels/Ocean: First, we define a shoreline with the opening angle method (27) on a binarized image where bed elevations below sea level were considered water and above sea level were considered land. We use an opening angle of 70°. All pixels not within

4 | Tejedor et al.

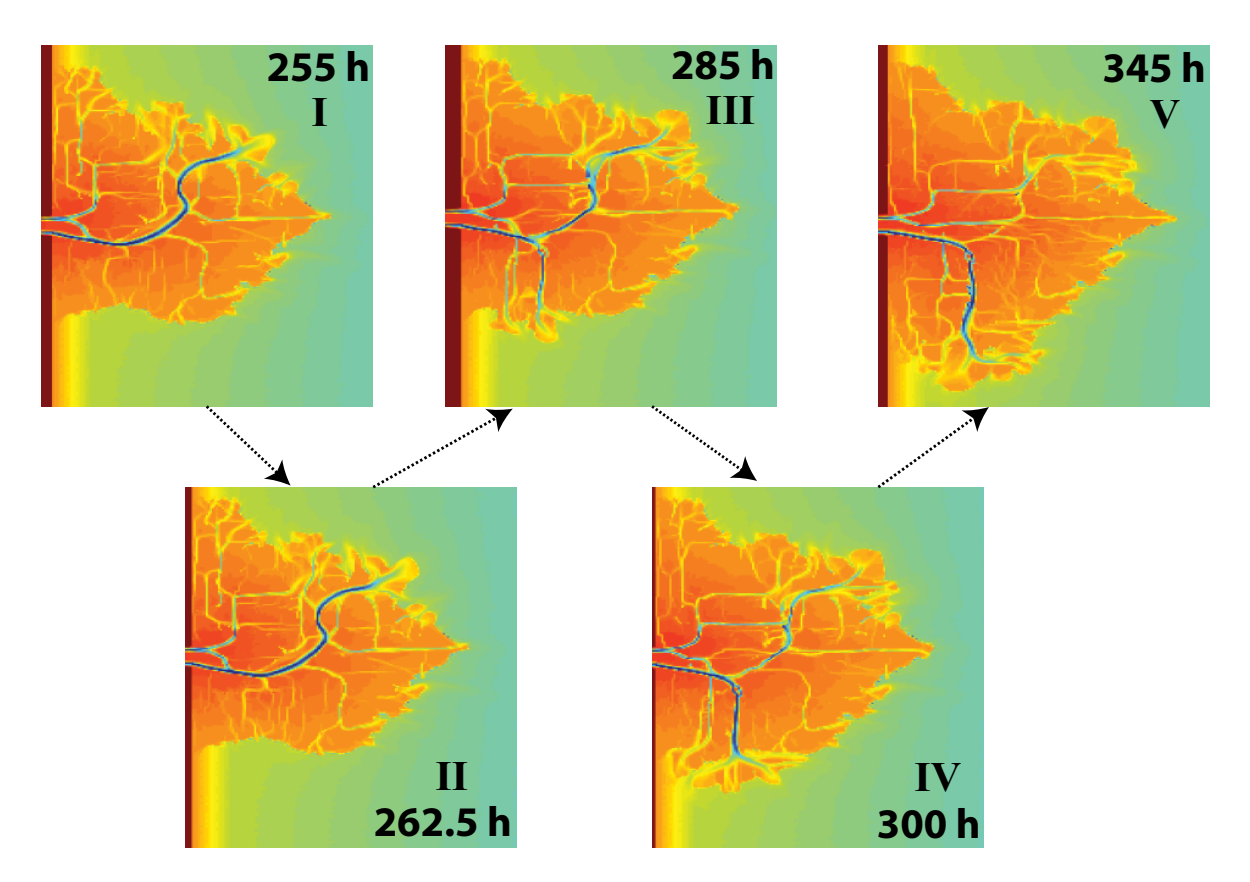


Fig. 4. Avulsion cycle. Five instances in an avulsion cycle of a Delft3D simulated delta where the main channel shifts, draining from the left (I) to the right (V) part of the delta shoreline. Intermediate stages of the avulsion cycle are also displayed: (II) the new path is created, (III) fluxes are equally divided between both paths, and (IV) the new path carries most of the flux. Top (bottom) panels are characterized by high (low) nER. Each panel is labelled with its corresponding time of simulation in hours (1 hr = 7.3 days morphodynamic time).

the shoreline are defined as ocean. Within the enclosed shoreline, pixels are defined as channels if depth >0.25 m, velocity >0.2 m  $\rm s^{-1},$  and sediment transport rate  $>2.25 \ \rm x \ 10^5 \ m^3 s^{-1}.$  Everything else within the shoreline is defined as land.

- 2. Eliminate disconnected channels: From all the channel pixels, we only consider those ones that belong to channel pathways that eventually drain from the apex to the shoreline, removing isolated pixels and paths.
- 3. Extract skeleton network: We use an algorithm (28) to define the centerline of each channel, taking into account that channels can have a large range of variation in widths (from one pixel to several). From the resulting skeleton structure and flow directions, we define the vertices and edges that uniquely determine the directed graph corresponding to the delta channel network [e.g., see Tejedor et al. (1), Figure 7].
- 4. Compute adjacency matrix: All information about the network connectivity can be stored in a sparse matrix called adjacency matrix. The element of the matrix  $a_{ij}$  is different from zero if the vertex j is directly connected to downstream vertex i, and zero otherwise.
- 5. Extract channel widths: The width of channels measured directly downstream of each bifurcation is stored and used

as a proxy for flux partition [see Tejedor et al. (1), section 2.2].

- Tejedor A, Longjas A, Zaliapin I, Foufoula-Georgiou E (2015) Delta channel networks: 1.
   A graph-theoretic approach for studying connectivity and steady state transport on deltaic surfaces. Water Resour Res 51:3998–4018.
- Smart J, Moruzzi V (1971) Quantitative properties of delta channel networks. Technical Report 3, IBM Thomas J. Watson Research Center pp 1–27.
- Edmonds D, Paola C, Hoyal D, Sheets B (2011) Quantitative metrics that describe river deltas and their channel networks. J Geophys Res 116:F04022.
- Syvitski J, Kettner A, Correggiari A, Nelson B (2005) Distributary channels and their impact on sediment dispersal. Mar Geol 222–223:75–94.
- Orton G, Reading H (1993) Variability of deltaic processes in terms of sediment supply with particular emphasis on grain size. Sedimentology 40:475–512.
- 6. Goudie A (2005) The drainage of Africa since the Cretaceous. *Geomorphology* 67:437–456.
- Politis G, Bonomo M, Castineira C, Blasi A (2011) Archaeology of the upper delta of the Parana river (Argentina): Mound construction and anthropic landscapes in the Los Tres Cerros locality. Quat Int 245:74–88.
- Fossati M, Cayocca F, Piedra-Cueva I (2014) Fine sediment dynamics in the Rio de la Plata. Adv Geosci 39:75–80.
- Nelson H, Creager J (1977) Displacement of Yukon derived sediment from Bering sea to Chukchi sea during holocene times. Geology 5:141–146.
- Walker H (1998) Arctic deltas. J Coastal Res 14:718–738.
- Hedley P, Bird M, Robinson R (2010) Evolution of the Irrawaddy delta region since 1850. Geogr J 176:138–149.
- Arnborg L, Walker H, Peippo J (1967) Suspended load in the Colville river, Alaska, 1962. Geogr Ann 49:131–144.
- Jorgenson M, Shur Y, Walker H (2010) Evolution of a permafrost-dominated landscape on the Colville River Delta, Northern Alaska eds. Lewkowicz A, Allard M. (Quebec, Canada), pp 523–529
- Roberts H, Coleman J, Bentley S, Walker N (2003) An embryonic major delta lobe: A new generation of delta studies in the Atchafalaya-Wax lake delta system. Gulf Coast Assoc Geol Soc Trans 53:690–703.
- Wagner W, et al. (2017) Elevation change and stability on a prograding delta. Geophys Res Lett 44:1786–1794.
- 16. Roberts H, Walker N, Cunningham R, Kemp G, Majersky S (1997) Evolution of sedimentary

- architecture and surface morphology: Atchafalaya and Wax lake deltas, Louisiana (1973-1994). Gulf Coast Assoc Geol Soc Trans 47:477–484.
- Paola C, et al. (2011) Natural processes in delta restoration: Application to the Mississippi delta. Annu Rev Mar Sci 3:67–91.
- Shaw J, Mohrig D, Whitman S (2013) The morphology and evolution of channels on the Wax lake delta, Louisiana, USA. J Geophys Res Earth Surf 118:1562–1584.
- Oosterlaan S, Meyers M (1995) Evolution of the Mossy Delta in Relation to Hydrodam Construction and Lake Level Fluctuation. (University of Illinois, Chicago), p 31.
- Smith N, Slingerland R, Perez-Arlucea M, Morozova G (1998) The 1870s avulsion of the Saskatchewan river. Can J Earth Sci 35:453–466.
- Bhattacharya J, Giosan L (2003) Wave-influenced deltas: geomorphological implications for facies reconstruction. Sedimentology 50:187–210.
- 22. Giosan L, Constantinescu S, Filip F, Deng B (2013) Maintenance of large deltas through

- channelization: Nature vs. humans in the Danube delta. Anthropocene 1:35-45.
- Lesser G, Roelvink J, van Kester J, Stelling G (2004) Development and validation of a threedimensional morphological model. Coastal Eng 51:883–915.
- Caldwell R, Edmonds D (2014) The effects of sediment properties on deltaic processes and morphologies: A numerical modeling study. J Geophys Res Earth Surf 119:961–982.
- Van Rijn L (1984) Sediment transport: Part I, Bed load transport. J Hydraul Eng 110:1431– 1456.
- Van Rijn L (1984) Sediment transport: Part II, Suspended load transport. J Hydraul Eng 110:1613–1641.
- Shaw J, Wolinsky M, Paola C, Voller V (2008) An image-based method for shoreline mapping on complex coasts. Geophys Res Lett 35:L12405.
- Lam L, Lee SW, Suen C (1992) Thinning methodologies a comprehensive survey. IEEE Trans Pattern Anal Mach Intell 14:869–885.

6 | Tejedor et al.